Nanoscale

Accepted Manuscript

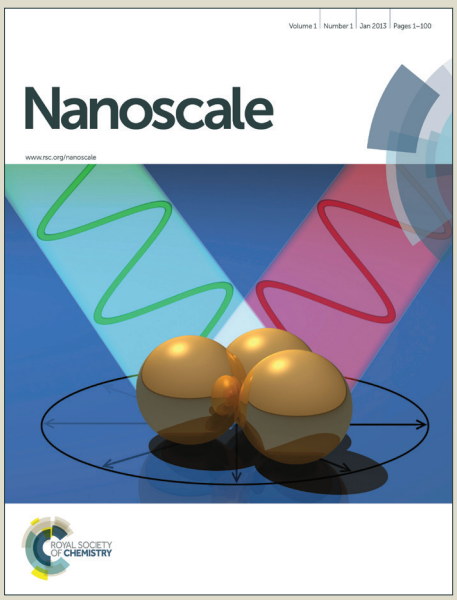

ROYAL SOCIETY OF CHEMISTRY

www.rsc.org/nanoscale

Nanoscale

RSCPublishing

ARTICLE

Role of zinc interstitials and oxygen vacancies of ZnO in photocatalysis: A bottom-up approach to control the defect density

Cite this: DOI: 10.1039/x0xx00000x

Received 00th March 2014,
Accepted 00th March 2014

DOI: 10.1039/x0xx00000x

www.rsc.org/

Fatma Kayaci,[a,b] Sesha Vempati,*[a] Inci Donmez, [a,b] Necmi Biyikli[a,b] and Tamer Uyar*[a,b]

Oxygen vacancies (V_Os) in ZnO are well known to enhance the photocatalytic activity (PCA), despite of various other intrinsic crystal defects. In this study we aim to elucidate the effect of zinc interstitials (Zn_i) and V_Os on the PCA, which has applied as well as fundamental interest. In order to achieve this one needs to overcome the major hurdle of fabricating ZnO with controlled defect density, where it is acknowledged that the defect level control in ZnO significantly hard. In the present context, we have fabricated nanostructures and thoroughly characterized for their morphological (SEM, TEM), structural (XRD, TEM), chemical (XPS) and optical (PL) properties. To fabricate the nanostructures, we have adopted atomic layer deposition (ALD), a powerful bottom-up approach. However to control defects, we have chosen polysulfone electrospun nanofibers as a substrate on which non-uniform adsorption of ALD precursors is inevitable due to the differences in the hydrophilic nature of the functional groups. For the first 100 cycles, Zn_i are predominant to yield ZnO quantum dots (QDs), while the presence of V_Os is negligible. As the ALD cycle number increases V_Os are introduced whereas the density of Zn_i is unchanged. We have employed photoluminescence (PL) spectra to identify and quantify the density of each defect for all samples. PCA studies are performed on all samples, and the percent change in the decay constant for each sample is juxtaposed with the relative densities of Zn_is and V_Os. A logical comparison on the relative defect densities of Zn_i and V_O suggested that the former are less efficient than the latter. This is because of the differences in the intrinsic nature and physical accessibility of the defects, while other reasons are elaborated.

Introduction

Photocatalysis in the presence of wide band gap semiconductors is a widely researched energy efficient approach for cleaner environment in which organic pollutants can be disintegrated.[1-3] However to increase the efficiency of a semiconductor catalyst one needs to isolate [4] or at least delay the recombination of photogenerated *electron* and *hole*.[1,5-13] To achieve this, lattice defects are induced in the semiconductor [1,6,8-13] apart from the fabrication of heterojunctions (either with noble metals [5-7] or another semiconductors [4,14]). In connection to the lattice defects, depending on the type and energetic location of the defect, their character is determined to capture either an *electron* or a *hole*, thereby the recombination process is delayed.[1-4,6,8-13] As a consequence the captured or free charge carrier participates in the photocatalytic activity (PCA), in which the catalysis takes place at conduction band (CB), valance band (VB) and the defect site if available on the surface.[4,8] Also note that the defects form intermediate bands within the band gap which allow the visible light harvest especially in the case of wide band gap semiconductors.[1,4,8,15-17] The lattice defects connected to PCA are basically intrinsic (vacancies, interstitials, anti-site) or extrinsic (induced by impurities) in nature.[1,4,6,8-13,15,18] However, it is rather hard, though intriguing to determine which defect is more beneficial for PCA, especially in the context of ZnO, as controlling the defect density and maintaining a balance among various types is quite challenging.[15] On the other hand, dominating defect density can compromise the optical quality, nevertheless, it increases the PCA as shown by us recently.[8]

Among various catalysts, the suitability of ZnO enables its major involvement in photocatalysis,[4,6,8,13,19-23] due to easy fabrication of nanostructures [21,22,24] ability to harvest UV through visible light of solar spectrum if appropriately doped. The defects associated with ZnO within the band gap are either donor type zinc interstitials (Zn_i^{++}, Zn_i^{+}, Zn_i^{*}) and oxygen vacancies (V_O^{++}, V_O^{+} and V_O) or acceptor type zinc vacancies (V_{Zn}'' and V_{Zn}').[25,26] Notably, the controllability of the defect density, of course depends on the type of defect and the semiconductor itself.[1,6,8-13] In the context of ZnO, vast amount of studies deal with V_Os [4,8,10,11,13,21] which is not the case with Zn_is. It is also notable that the balance between the relative densities of Zn_is and V_Os is still challenging.[15] The presence of Zn_i and V_O in ZnO can be easily identified through simple photoluminescence (PL) experiments [15-17,27] indicating blue and green emissions respectively. Notably, studies based on Zn_is are less frequent than V_Os as the former defects are difficult to achieve and control in as-prepared samples.[16,17,28-32] In contrast, typically synthesized ZnO is predominant with V_Os.[4,8,16,17,27,31,32] Consequently, the photocatalysis studies involving V_Os dominate the literature.[1,4,6,8-10,13,21] In this context, it is very useful and important to study the effect of Zn_is in the PCA and their efficiency against V_Os. Apart from the fundamental interest, the results of such a study enable an efficient and cost effective design of novel photocatalyst. As shown earlier,[33] Zn_is are very instable when compared to V_Os which are found to be stable even at 400 ˚C. After nearly two years,

theoretical support for this instability is given by Janotti et al.[34] where the authors suggest that Zn_is diffuse faster through a migration barrier as low as 0.57 eV, *cf* for V_Os it is from 1.7 to 2.4 eV. Since the ionization energies are in the range of 0.05 to 2.8 eV,[33] the formation temperature is detrimental for the relative concentrations of the various defects. One has to choose non-equilibrium processes to induce Zn_is [35,36] in which the samples were subjected to thermal annealing to control the density of the defects. Under oxygen deficient conditions at high temperatures V_Os are typical,[37] while Zn vapor-rich environments produce Zn_is.[38,39] As an example, when ZnO crystals are annealed in zinc vapor at 1100 ˚C, Zn_is are introduced into the lattice.[40,41] More recently Zeng et al.[15] followed an earlier reported method [35,36] in which zinc target is laser ablated in aqueous solution. The resultant colloids were subjected to thermal annealing in various atmospheres.[15] Apart from the above discussed methods [15,40,41] we will show that atomic layer deposition (ALD) can be employed to produce ZnO on polymer fibers consisting of Zn_is along with or without V_Os. The great control and precision of ALD [19,42,43] together with electrospun fibers yielded structures of ZnO with a clear transformation from quantum dots (QDs) to nanocoating (NC). The transformation is achieved simply by increasing the ALD cycles, during which the predominance transfers from Zn_is to V_Os while the density of the former is sustained for all cases. Notably, the earlier methods [15,35,36] require post thermal treatments to control the defect density, in contrast we have noticed predominantly Zn_i or Zn_i and V_Os in as-fabricated samples depending on the cycle numbers.

In this work, we have employed polysulfone (PSU) electrospun fibers as a substrate to deposit ZnO via ALD with varying deposition cycle numbers (*viz* 100, 200, 300 and 400). This variation has yielded ZnO quantum dots (100 cycles) dominating Zn_i related defects, while their probable origin is discussed. Further increase in the cycle numbers (≥ 300) has introduced V_Os in which case the density of Zn_is is more or less constant. The morphological transformation has shown significant variance in the crystal and optical properties of the samples. After thorough characterization (structural, optical and surface), the PCA is tested and juxtaposed against defect density. We believe that this study deepens the understanding of least studied crystal defect of ZnO, Zn_is in connection to their PCA.

Experimental

Materials

Polysulfone (PSU, M_w ~60,000) was purchased from Sp^2, Scientific Polymer Products, Inc. N, N-dimethylacetamide (DMAc, Sigma Aldrich, 99 %) was used as solvent. Methylene blue (MB, Sigma Aldrich, certified by the Biological Stain Commission) was employed in the catalysis study. In the ALD process, diethylzinc (DEZn, Sigma Aldrich) and HPLC grade water were used as zinc precursor and oxidant respectively. All materials were used as received.

Electrospinning of PSU fibers

PSU (35 wt %) in DMAc was rigorously stirred for 4 h at 60 °C to yield a homogeneous, clear yellowish solution. This solution when reached room temperature (RT) was taken into a syringe fitted with a metallic needle of 0.8 mm inner diameter. This syringe was fixed horizontally on a syringe pump (SP 101IZ, WPI) which was set to a feed rate of 0.75 mL/h. 15 kV bias was applied (Matsusada, AU Series) across the metal needle and the collector which were placed about 15 cm apart. The electrospun PSU fibers were collected onto an aluminum foil which was wrapped around a grounded metal electrode. The electrospinning process was performed in an enclosed chamber at 26 ˚C and 29 % relative humidity.

ALD of ZnO on electrospun fibers

PSU fibers were subjected to ALD reactor (Savannah S100 ALD reactor, Cambridge Nanotech Inc.) at 200 ˚C. Exposure mode (a trademark of Cambridge Nanotech Inc.) is employed to deposit ZnO, in which the pump valve was closed during the pulse steps and opened during the purge steps of the ALD cycle. Pulse times of the Zn-precursor and oxygen source were both 0.015 s, which were waited in the chamber for 10 s. Then, pump valve was opened for purging using N_2 at a flow rate of 20 sccm for 10 s. Using this procedure 100, 200, 300 and 400 ALD cycles were deposited. For the thickness estimation, same recipe and cycles were applied to a clean Si wafer.

Characterization

Scanning electron microscopy (SEM, FEI – Quanta 200 FEG) is performed on pristine PSU and ZnO coated PSU (PSU-ZnO) fibers after 5 nm thick Au-Pd sputter coating. Average fiber diameter (AFD) was calculated by measuring nearly 100 fibers from the SEM images. Spectroscopic ellipsometry (SE, Variable Angle Spectroscopic Ellipsometer, VASE© J.A. Woollam Co.) was employed to determine the thicknesses of the ZnO films on Si/SiOx wafer. SE spectra from ZnO films on Si/SiOx substrate were recorded at three angles of incidence (65˚, 70˚ and 75˚) within the wavelength range of 450-1200 nm. Cauchy dispersion function was employed to estimate the thickness of the ZnO film via $Si/SiO_2/ZnO$ model where the native oxide thicknesses of the Si substrates were measured through SE spectra. XRD patterns from pristine PSU and PSU-ZnO samples were obtained within the range of $2\theta = 10^o$-90^o by using PANalytical X'Pert Multi Purpose X-ray Diffractometer with Cu Kα radiation. Transmission electron microscopy (TEM, FEI – Tecnai G2F30) is also performed on the PSU-ZnO fibers, for which the fibers were dispersed in ethanol and a tiny droplet is dried on a holey carbon coated TEM grid. Selected area electron diffraction (SAED) patterns were also recorded. The surface composition of pristine PSU and PSU-ZnO fibers were determined via X-ray photoelectron spectroscope (XPS, Thermoscientific, K-alpha) equipped with a monochromated Al K_α X-ray source ($h\nu$ = 1486.6 eV) and flood gun charge neutralizer system. Avantage software is employed for the deconvolution of various peaks. Horiba Scientific FL-1057 TCSPC was used for the PL measurements performed at an excitation wavelengths of ~320, 330 or 350 nm. The interband transition is taken as reference and each of the spectra was normalized individually. Then these spectra were subjected to the deconvolution using Origin 6.1. The thermal properties of the PSU and PSU-ZnO fibers were investigated via thermogravimetric analyzer (TGA, Q500, TA Instruments) from RT to 700 ˚C at a heating rate of 20 ˚C/min under N_2 flow.

Photocatalytic activity of the PSU-ZnO fibers

MB aqueous solution (18.8 μM) is the subject for the investigation of PCA of the PSU-ZnO fibers, and compared with the pristine and no catalyst cases. The samples (~11 mg) were immersed into MB solution in quartz cuvettes and exposed to UV irradiation (8 W, UVLMS-38 EL, 365 nm) from a distance of ~10 cm. The PSU and PSU-ZnO fiber were at the bottom of the cuvette during the experiment, and therefore did not interfere with the measurement. As a control experiment, the MB solution without any catalyst was subjected to the same UV treatment in order to compare with the catalyst case. The changes in the absorption peak of MB at 665 nm as a function of UV-irradiation time (t) were analyzed via UV-Vis-NIR spectrophotometer (Varian Cary 5000). The concentrations of

MB before and after UV irradiation are defined as C_0 and C respectively. The rate of dye degradation (C/C_0) is quantified with first order exponential fit ($y = y_0 + \alpha\, e^{-x/\tau}$) for each sample with an automated routine in Origin 6.1, where α-pre exponential factor, x-time axis, y- C/C_0 at different 't' and τ-decay constant. All the parameters are set as free (unless otherwise stated) until convergence.

Results and discussion

PSU-ZnO fibers were fabricated via two-step process in which electrospinning is followed by ALD with varying cycle numbers (Fig. 1). In the first step (Fig. 1a), bead free PSU fibers were produced and then transferred to an ALD chamber (Fig. 1b) to deposit ZnO for 100, 200, 300 or 400 ALD cycles. By varying the number of cycles, we have achieved QDs or NC on PSU fibers (Fig. 1c). The PSU-ZnO samples obtained using various cycle numbers *viz* 100, 200, 300 and 400 ALD cycles will be referred as PZ1 QD, PZ2 NC, PZ3 NC and PZ4 NC respectively. As we go along we will see that this nomenclature is quite appropriate for each sample.

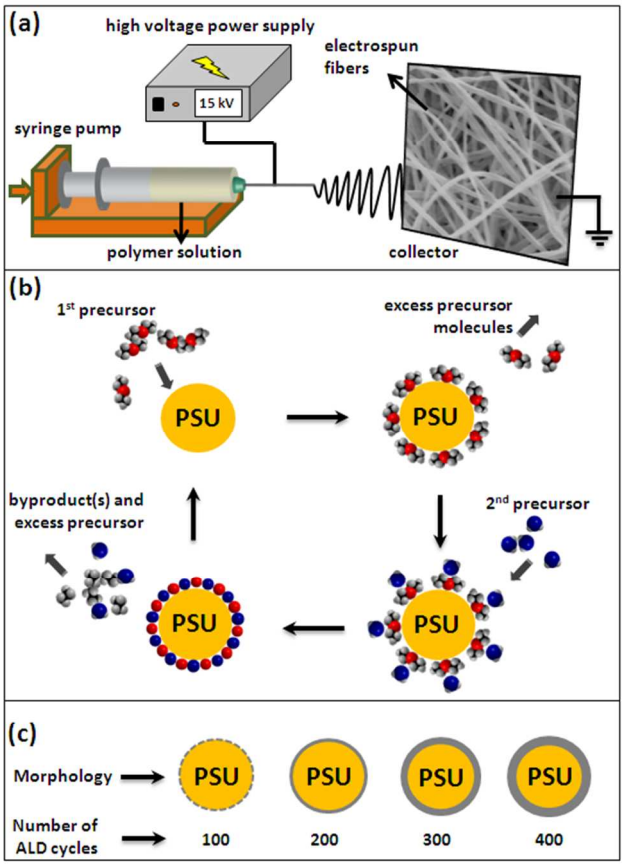

Fig. 1 Schematic of (a) electrospinnig, (b) atomic layer deposition (ALD) and (c) the resultant morphology of the samples obtained applying different ALD cycle numbers.

Polymeric structure can be easily deformed or degraded under the deposition of other materials via conventional chemical vapor deposition,[44] which require elevated temperatures. In contrast, ALD uses relatively lower temperature in which the substrate is exposed to two or more precursors separated by purging/evacuation periods (Fig. 1b). Notably, ALD is a powerful tool to deposit ZnO and/or other inorganic layers on polymeric films [45] and fiber mats.[45-47] In this process the substrate is exposed to gaseous precursor molecules which do not react with themselves, and new surface sites are formed for the following precursor pulse.[48] The morphology of the pristine PSU and PSU-ZnO fibers was investigated via SEM. The optimized electrospinning parameters yielded bead-free fibers although the surface of the fiber is noticeably rough (Fig. 2a). After the ALD processing we have recorded SEM images for all cycle numbers and shown in Fig. 2b-e. The fibers retained their structure after the ALD process in all cases, where it is notable that compatibility between the precursor and the substrate is vital.[45,49]

The initial stage of transformation of QDs into NC can be seen from the inset of Fig. 2c, where the grains of ZnO are explicit. The AFDs of the PSU and PSU-ZnO fibers are summarized in Fig. 2f and an obvious increase in the fiber diameter is noticed for higher ALD cycles, as expected. However, by given the standard deviation in the diameter measurement, we have estimated the thickness of the ZnO coating by other methods which will be discussed later.

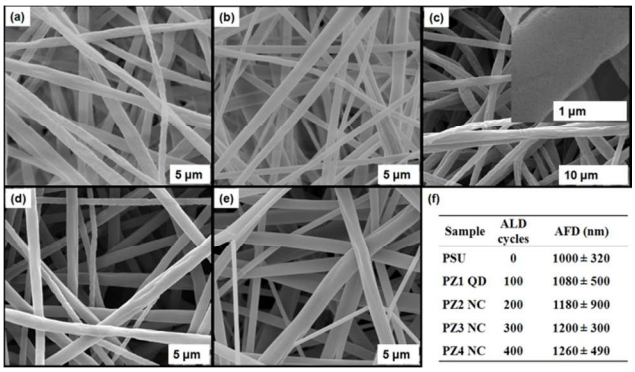

Sample	ALD cycles	AFD (nm)
PSU	0	1000 ± 320
PZ1 QD	100	1080 ± 500
PZ2 NC	200	1180 ± 900
PZ3 NC	300	1200 ± 300
PZ4 NC	400	1260 ± 490

Fig. 2 SEM images of electrospun fibers of (a) pristine PSU, (b) PZ1 QD, (c) PZ2 NC, (d) PZ3 NC, (e) PZ4 NC and (f) average fiber diameters.

The morphologies of the PSU-ZnO fibers were further investigated by TEM (Fig. 3). Fig. 3a shows the QD formation on the surface of PSU fibers for 100 ALD cycles. In this sample, highly-dense ZnO QDs with an average diameter ~10 nm were homogenously distributed on the fiber surface (Fig. S1 of ESI). When the number of cycles was increased, the process yielded a continuous ZnO coating on PSU fibers of uniform thickness, *viz* for 200, 300 and 400 cycles see Fig. 3b, c and d, respectively. Note the dark region at the edge of the fiber which represents the ZnO coating gets thicker with increasing ALD cycles. Therefore, ALD process with sufficient cycle numbers yielded conformal and layer-by-layer deposition of ZnO on PSU fibers.[4,19,20,49] For cycle numbers ≥ 200, a continuous film is formed due to the coalescence of grains/islands. Fig. 3e shows high resolution TEM image of PZ4 NC, where we can see the lattice fringes as well as grains grown in different lattice directions (see double arrows on figure). This grainy structure is consistent with the earlier observation for less number of ALD cycles. Left inset of Fig. 3e shows the lattice resolved image with a lattice spacing of ~2.23 nm, which represents the *c*-axis of ZnO. Furthermore SAED pattern from PZ4 NC is shown as right inset of Fig. 3e, which indicates a polycrystalline sample. The diffraction planes are annotated on the image and found to be consistent with the literature.[16,32] Furthermore, we have measured the thickness of ZnO coating from TEM images and determined to be ~43, 56 and 75 nm for PZ2 NC, 3 NC and 4 NC, respectively. The ZnO shell thicknesses as a function of ALD cycle numbers are shown in Fig. S2 of ESI for two contexts, namely, PSU-ZnO fibers and ZnO coating on silicon wafer. The former case is from TEM image

analysis, while the latter from SE. We can see the consistency in both the methods, meaning the conformal coating of ZnO on the surface of the polymer fibers. Note that the thickness of the ZnO-shell on the fibers for 100 ALD cycles is not shown as it forms island like structure than a continuous film. A linear fit for the data points from TEM analysis yielded a growth rate of 0.20 nm/cycle where ALD should be acknowledged for the excellent control on the film thickness against deposition cycles.[19,42,43] On the other hand, SE from Si yielded 0.18 nm/cycle which is closely comparable with the results from TEM.

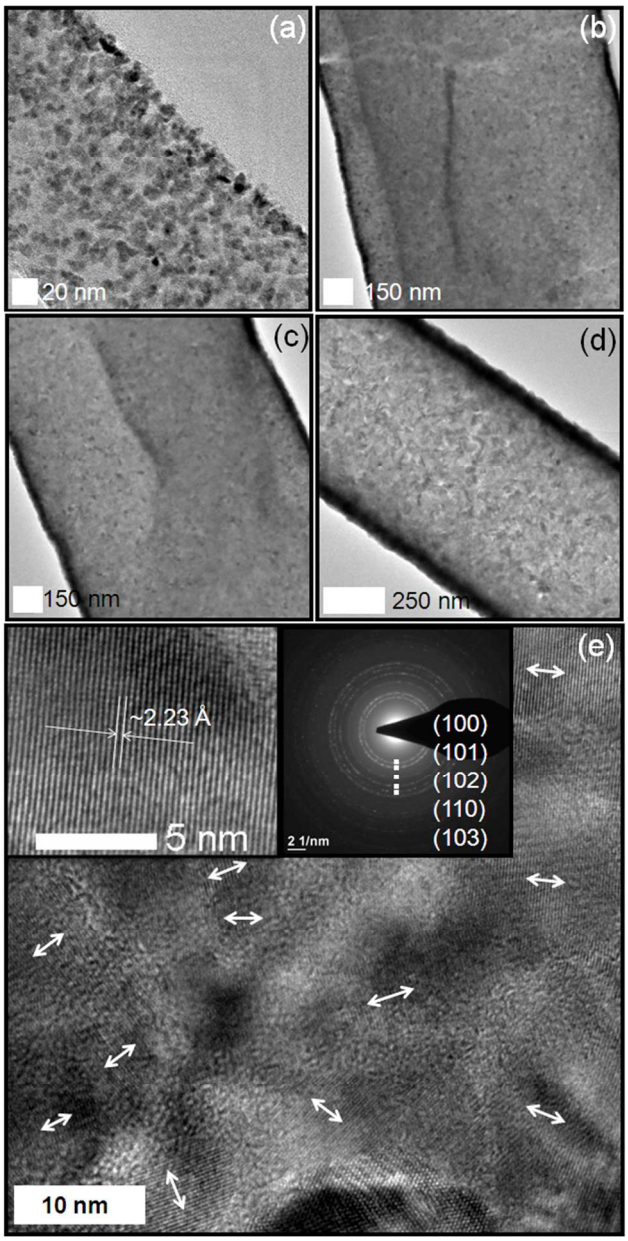

Fig. 3 TEM images of (a) PZ1 QD, (b) PZ2 NC, (c) PZ3 NC and (d) PZ4 NC; (e) high resolution images and electron diffraction pattern from PZ4 NC.

Fig. 4 shows the XRD patterns from PSU-ZnO fibers of varying cycle numbers. Broadly, the diffraction peaks of ZnO were found to be wurtzite structure for all cases. Reflections corresponding to ZnO, *viz* (100), (002) and (101) planes (30-38˚) are annotated as (i), (ii) and (iii) respectively and shown on Fig. 4a. We observed that as the cycle number increases the peaks became sharper (see full width at half maximum, *fwhm* in Table S1 of of ESI) and more well defined. As we can see from Fig. 4a (also see Table S1 of ESI) a significant shift (δ°) is observed for all the three peaks (ICDD 01-074-0040).[16,32] In an earlier report [15] the authors have observed similar shift for (100) peak from the normal, where the shift is attributed to lattice defects. As outlined in the introduction we are interested in creating defects related to Zn_is, on the other hand, we note that lattice has gone through a 'strain' induced by defects. Hence it is important to establish if we can expect defects of Zn_i origin in the present samples. In the earlier study,[15] the defects are induced by non equilibrium process, which are sensitive to temperature and can only withstand low temperature annealing.[50] Vlasenko et al. suggested that Zn_is are not stable unlike V_Os which are stable up to ~400˚C.[33] In line with this, results from a simulation study also suggested that Zn_is diffuse faster than V_Os where the migration barriers are 0.57 eV and 1.7 to 2.4 eV, respectively.[34] While keeping this in the background, we can see that the other reflections, (002) and (101) have also shown some nonlinear deviation. These features indicate that the as-prepared samples (PSU-ZnO) are rich in some kind of defects induced during the ALD process. Since the present deposition temperature is about 200˚C, the defects such as Zn_is are stable as shown by other researchers.[33,34] As we go along we will see that these defects are actually interstitial zinc. Various other diffraction planes within 45-90˚are annotated on Fig. 4b and found to be consistent with the literature.[16,31,32]As the cycle number increases (300 and 400) we can see that the peaks (200), (112) and (201) have been evolved to be clearer and well-defined when compared to PZ1 QD and PZ2 NC samples. Furthermore, we have also observed a single peak for pristine PSU at 17.9˚ due to the semi-crystalline nature of the PSU fibers (Fig. S4 of ESI). As the cycle number increases, this peak is relatively extinguished (not shown here) as it is screened by the inorganic (ZnO) coating. However, it is notable that ALD did not significantly influence the crystalline nature of PSU, where we note the deposition has taken place at 200˚C.

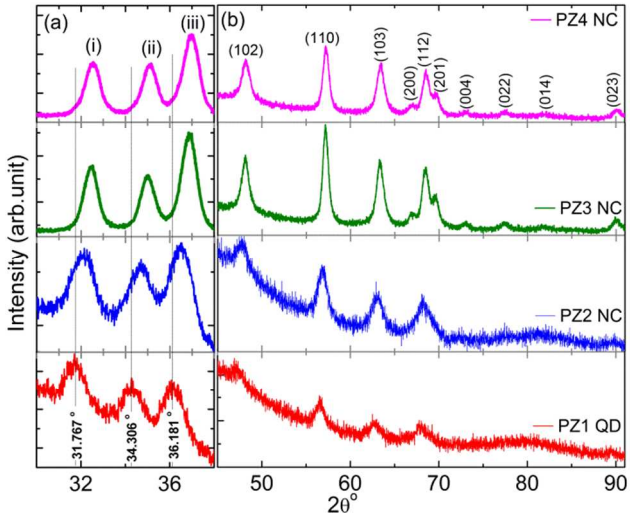

Fig. 4 XRD patterns from PZ1 QD, PZ2 NC, PZ3 NC, and PZ4 NC within (a) 30-38˚and (b) 45-90˚regions.

The core-level XPS spectra of O 1*s* and Zn 2*p* are shown in Fig. 5 and Fig. 6 respectively. O 1*s* spectra have been deconvoluted for all the cases depending on the chemistry of the surface. The spectral location of the deconvoluted peaks match with the literature.[51]

Pristine PSU has shown two principle peaks corresponding to two oxygen molecules in different chemical environment (O/S and O/C) where O/S and O/C represent the oxygen bonded to sulfur or carbon respectively (Fig. 5a).[51] In PZ1 QD sample we can observe oxygen from ZnO (O/Zn) and PSU owing to the absence of continuous ZnO layer on the PSU fibers as evidenced from TEM images. All the deconvoluted spectra suggested the presence of chemisorbed oxygen (O_{Ch}, shaded area on the figure). This O_{Ch} can be from any of the species such as –OH, –CO, adsorbed H_2O and/or O_2 (ref. [4,8,52,53]) or O^- and O^{-2} ions.[4,8] The area under the peak corresponding to O_{Ch} is annotated on the image. If we keep aside the O_{Ch} of PSU, the origin of such species for the PZ1 QD is at higher binding energy than the other PSU-ZnO cases. This is not surprising because ZnO has not completely covered the surface of PSU which means that the peak in the spectrum is the sum of two contributions. O_{Ch} from PZ1 QD has shown an area of 0.28 eV·cps, while the other PSU-ZnO samples have shown an average value ~0.42 eV·cps. In the case of ZnO, the quantity of O_{Ch} is a measure of V_Os,[4,8,32] as the former occupies the place of the latter in the lattice. Hence the density of V_Os is increased with the thickness of ZnO or with the ALD cycle numbers (≥ 200). We will refer to the density of V_Os and their effect on emission properties in the context of PL.

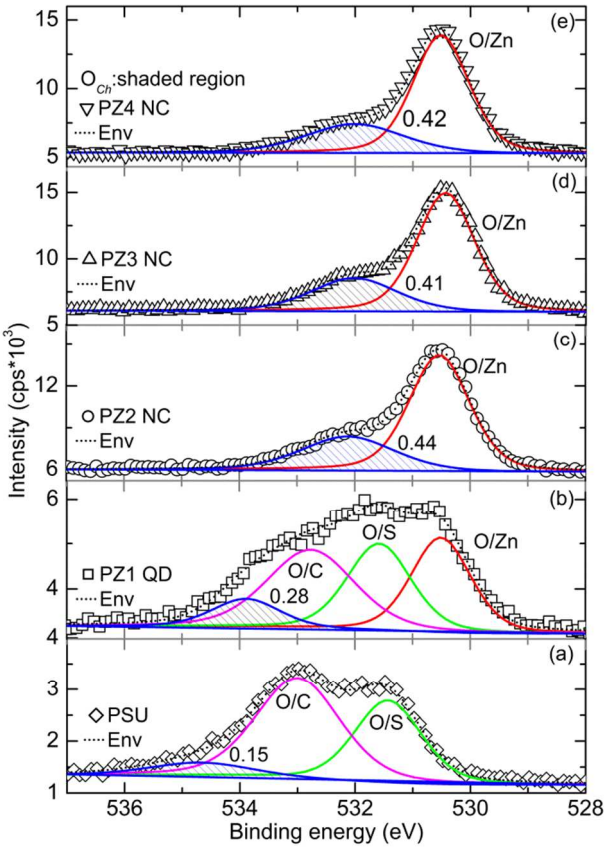

Fig. 5 Core-level XPS analysis for O 1*s* from PSU, PZ1 QD, PZ2 NC, PZ3 NC and PZ4 NC samples. The area under the shaded peak corresponding to chemisorbed oxygen (O_{Ch}) is annotated on the image in the units of eV·cps.

Zn 2*p* core level spectrum is important to study, especially when we suspect the interstitial defects related to zinc. The spectra in Fig. 6 are broadly similar across all samples and the spectral position of each peak is consistent with literature conforming the formation of ZnO.[51] However, a closure inspection of spectrum from PZ1 QD sample has shown shoulder like feature at higher energy side of Zn $2p_{3/2}$ and Zn $2p_{1/2}$ peaks (see the shaded area in Fig. 6a). The energetic location of these shoulders (1024.19 and 1047.11 eV) suggests that the zinc is in its more oxidized form than ZnO. Note that this does not correspond to Zn $(OH)_2$, in which case $2p_{3/2}$ peak should occur in between 1022.70-1021.80 eV.[51] This is an important observation, where the Zn atom has taken an interstitial site and surrounded by more than one oxygen atoms at the same time. This can be treated as a direct evidence for the presence of Zn_is and on the other hand, we may also expect some V_{Zn} defects about which we will discuss in the context of PL in detail.[15] We did not see any shoulder or like features in the spectra of Zn 2*p* from PZ2 through PZ4 NC samples (Fig. 6b, c and d). We believe that the surface adsorption during the ALD process has taken its toll and shown a significant effect. Initially, DEZn is adsorbed on the surface of PSU and then H_2O vapor arrives to react. However, the adsorption of H_2O on the surface of PSU is not uniform, as it has two functional groups one of which is more hydrophilic (O=S=O) than the other (C-O-C). Hence the molecular adsorption of H_2O varies from place to place on the surface. As the cycle number increases, the surface is coated with ZnO which leads to the change in the surface chemistry and we can expect more uniform adsorption of precursor molecules. In the initial cycles, the uneven distribution of molecules on the surface of PSU would have caused the growth of ZnO with dominating Zn_i related defects. Nevertheless, it does not necessarily mean that Zn_is are not present for the higher cycle numbers, as we will see in the context of PL. However the lack of signal from Zn_is might be due to increased Zn signal contribution from ZnO.

In the discussion of O_{Ch} (or V_Os), it is noted that PZ1 QD possesses the least amount of V_Os while Zn 2*p* analysis suggests that it has higher amount of Zn_i related defects. As the thickness of ZnO coating increased (≥ 200 ALD cycles) Zn_i related defects were not detected, while simultaneously O_{Ch} signal was increased. Finally, for the first 100 ALD cycles Zn_is are seen with limited V_Os; as the thickness of ZnO increases, although the presence of Zn_is is not explicit, the density of V_Os is definitely increased. In other words, V_Os and Zn_is are predominant in thicker and thinner coatings, respectively.

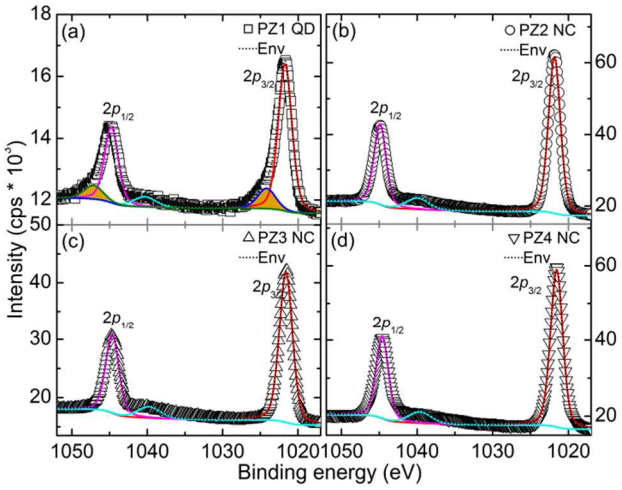

Fig. 6 Core-level XPS analysis for Zn 2*p* from PZ1 QD, PZ2 NC, PZ3 NC and PZ4 NC samples.

The PCA of any semiconductor can be understood by carefully analyzing the optical properties [4,8] where the information about the radiative recombination centers (other than CB) associated with

crystal defects would be revealed. In principle, there are a number of defect states within the band gap of ZnO. The donor defects are Zn_i^{+}, Zn_i^{++}, Zn_i^{*} (neutral), V_O^{++}, V_O^{++}, and V_O^{*}(neutral), and the acceptor defects are V''_{Zn} and V'_{Zn}.[25,26] Zn_is and V_Os are known to be the predominant ionic defect types,[16,31,54-56] where the former are shallow donors, while the latter create deep levels.[17,54,56] At higher oxygen partial pressures V_{Zn} and O_i may also be thermodynamically stabilized.[55] However, which defect (Zn_i or V_O) dominates in native, undoped ZnO is still under debate.[15] To emphasize, in the present case, the density of Zn_i is controlled by simply altering the ALD cycle numbers for which researchers have used non-equilibrium processes [15,35,36] followed by thermal annealing to control the defect density, in contrast we will see that as prepared samples possesses defects such as Zn_is. Zn_is come from Frenkel reaction, Eq (1), and further ionization reactions, Eq (2) and (3).

$$Zn_{Zn} \Leftrightarrow Zn_i^{*} + V_{Zn}^{*} \quad (1)$$
$$Zn_i^{*} \Leftrightarrow Zn_i^{+} + e^{-} \quad (2)$$
$$Zn_i^{+} \Leftrightarrow Zn_i^{++} + e^{-} \quad (3)$$

Blue emission from ZnO nanoparticles has been explained earlier by H. Zeng et al.[15] in which Zn_i are at the core of the emission. Furthermore, extended states of Zn_i (ex-Zn_is) can be formed according to the defect ionization reaction, equations (2) and (3), and can result in defect localization coupled with a disordered lattice. It is notable that blue emissions are quite infrequent [15] for the as-prepared samples when compared with the literature.[16,17,28-32] To note, Zn_i is 0.22 eV below the CB,[57] V_{Zn} is 0.30 eV above the VB [58-60] and ex-Zn_is are 0.54 to 0.635 eV below the CB[15] in ZnO for a typical band gap of 3.36 eV.[16] As mentioned earlier, the other set of major defects are V_Os, which have been addressed in the literature extensively, see the discussion and cross-references in Ref [16]. Despite of various interpretations, previous studies [17,27] are found to be rather useful in which the energetic location of V_Os has been confirmed through an indirect method. Based on this, V_O^{+} state captures an *electron* from CB and forms a neutral state (V_O^{*}), from which a transition to VB takes place emitting green light of ~500 nm wavelength, Eq (4).[16,17,27] On the other hand, V_O^{+} captures a *hole* from VB and forms a V_O^{++} state into which an *electron* recombines from CB and emits green light of ~565 nm wavelength, Eq (5).

$$V_O^{*} \Leftrightarrow V_O^{+} + e^{-} \quad (4)$$
$$V_O^{++} \Leftrightarrow V_O^{+} + h^{+} \quad (5)$$

To note, V_O^{*} is ~0.86 eV below the CB and V_O^{++} is 1.16 eV above the VB,[27] for a typical band gap of 3.36 eV with an exciton binding energy of 60 meV.[16] The processes described in Eq (4) and (5) take place in bulk grain region (BGR) and depletion region (DR) respectively.

Based on the above discussed defects and their energetic location within the band gap, the present PL spectra were deconvoluted and shown in Fig. 7a and the possible emission mechanism is schematized in Fig. 7b. Emissions from ZnO, $a_{1\text{-}4}$, $b_{1\text{-}4}$, $c_{1\text{-}4}$, $d_{1\text{-}4}$ and $e_{1\text{-}4}$ in Fig. 7a correspond to the transitions *a*, *b*, *c*, *d*, and *e* in Fig. 7b. The spectral location of each peak (in eV and nm) is tabulated in Table 1, along with the emission mechanism. Before we discuss about the various emission lines, it would be appropriate to mention about the fluorescence peak of PSU, from PZ1 QD sample on which the ZnO coating is not continuous. We have employed 350 nm excitation (λ_{Ex}) for analyzing the emission from ZnO for which PSU has shown a shoulder like structure; see the normalized emission spectra for three different excitations in Fig. S4 of ESI. By considering the shape of the emission, Lorentzian fit is employed for PSU, and we can see a perfect retrace of the data points on Fig. 7a (top left panel), which peaked at ~363 nm (*P'*) for 320 nm excitation. Keeping this in the background, in the case of PZ1 QD, during the deconvolution the spectral location of this peak is fixed (*P''*) and the other parameters are allowed vary, where the excitation wavelength is 350 nm. As mentioned earlier, in the case of ZnO, the peak attributions and their wavelengths are still under severe discussion,[15] however, the present assignments were performed based the available evidence in the literature while placing a logical approach for the cases where more than one transition is feasible. Also refer to the schematic diagram Fig. 7b, for each transition that is described below.

The least controversial emission from interband transition occurred in the range of 382-390 nm ($a_{1\text{-}4}$) for all samples, where an *electron* from free exciton (FX) level recombines with a *hole* in VB. The blue region of the emission contains two probable transitions related to V_{Zn} and Zn_i, i.e. *electron* from CB recombines with the *hole* at V_{Zn} or an *electron* is captured by Zn_i then recombines with *hole* in VB. Either or both of these transitions take place emitting $b_{1\text{-}4}$.[16,57,58] After a careful inspection it appears to be the case that the observed emission ($b_{1\text{-}4}$) should be ascribed to $Zn_i \rightarrow$VB transition, as we have noted interstitial zinc in the XPS, at least for PZ1 QD case. In 2010 a study by Zeng et al.[15] introduces probable transitions from Zn_i or ex-Zn_is to the VB, while an earlier investigation in 2009 by Ahn et al. which suggests transitions form Zn_i to V_{Zn} states.[57] Further complicating the attribution, in our case both the arguments have a reasonable over lap within blue wavelength region, $c_{1\text{-}4}$ (Table 1). In the discussion given by Zeng et al,[15] *electrons* from CB are relaxed to Zn_i (in line with Ahn et al.[57]) and/or ex-Zn_i via non-radiative process and then to VB via emitting violet and/or blue emissions respectively. On the other hand, Ahn et al.[57] suggest two transitions from Zn_i to VB and/or V_{Zn}, nevertheless, in the present context this description might not be feasible, because as we have evidenced Zn_is through XPS. Hence the peaks, $c_{1\text{-}4}$, are attributed to ex-Zn_i to VB transition, as the dominant Zn_is can form extended states. Finally, the green emission occurs due to V_Os constituting two transitions [17,27,32] as shown in Table 1. These transitions are annotated with $d_{1\text{-}4}$ and $e_{1\text{-}4}$ in the Table 1 fall within 498-501 nm and 562-566 nm, respectively. The spectral locations of all of the above mentioned peaks are quite consistent with the literature.[4,15-17,31,32] It is clear that the present samples possess defects such as Zn_is and V_Os, however, in the following we will consider the relative densities (integrated area of the peak) of each transition that is ascribed in Table 1 while referring to Table S2 of ESI. Such comparison is found to be very useful by us in explaining the PCA earlier.[4,8]

To start with, $a_{1\text{-}4}$ are supposed to be sharp and intense for defect free ZnO,[16] also see cross-references therein. However in the present case the *fwhm* does not vary significantly across all samples. While the area under the peak (*A*) seemed to improve from PZ1 QD to the rest of the samples indicating slightly improved optical quality.[16,31,32] The next region to consider is violet emission, $b_{1\text{-}4}$, where the *fwhm* is almost same for all samples. Further, PZ1 QD has shown lowest *A*, which nominally increased with the ALD cycle numbers. The blue emission, $c_{1\text{-}4}$, has shown interesting features, where the *fwhm* is almost similar for all sample, in contrast *A* is almost twice for PZ1 QD when compared to other PSU-ZnO samples. It will be more contextual to discuss the reason for this difference after addressing the rest of the emissions. We can see that *fwhm* of $d_{1\text{-}4}$ increased with the ALD cycle numbers while, *A* is comparable among the samples set wise, PZ1 QD and PZ2 NC; PZ3 and PZ4 NC. In the case of PZ1 QD and PZ2 NC the thickness of the ZnO is not more than ~40 nm, while the transitions d_1 and d_2 take place in the BGR. Since the grains are not completely formed for such thicknesses, the intensity of the transition is comparatively low. In the context of d_3 and d_4, there is a significant increase in the thickness which has led to the formation of high density BGRs emitting relatively higher intensity green light, thereby higher *A*.

Peak *e* occurs from the DR, in which case the argument given for d_{1-4} is still valid (Fig. 7b). At lower thickness values, the density of V_Os is relatively less, especially with PZ1 QD. Thereby it is clear that the capture of electrons by V_O^+ state is almost negligible; hence a predominant emission is noticed for c_1 with *A* value of ~67 nm·counts which is almost the double intensity of c_{2-4}.

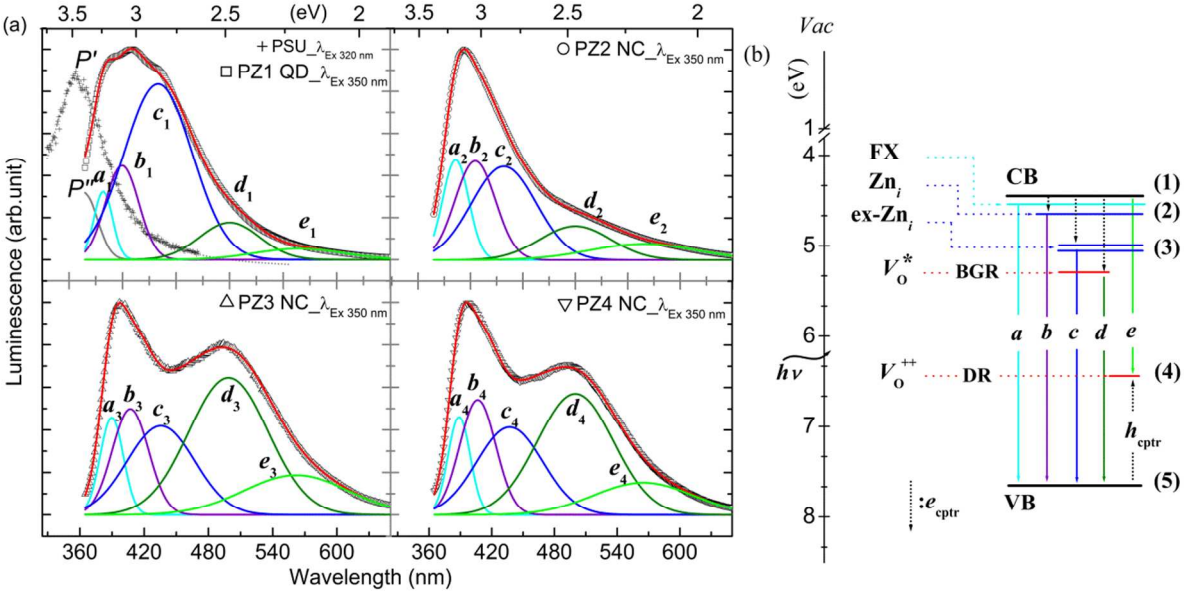

Fig. 7 (a) Luminescence spectra from electrospun fibers of PSU and PZ1 QD, PZ2 NC, PZ3 NC, and PZ4 NC. Spectrum from PSU is co-plotted with that of PZ1 QD for 320 nm excitation with Lorentzian fit. Spectra from PSU-ZnO samples are decomposed into Gaussian peaks. (b) Schematic diagram depicting the various defects and the ascribed transition, where a_{1-4}, b_{1-4}, c_{1-4}, d_{1-4} and e_{1-4} in (a) correspond to the transitions *a*, *b*, *c*, *d*, and *e* in (b). FX and Zn_i are 0.06 eV and 0.22 eV below the CB respectively,[57] while ex-Zn_is are 0.54 to 0.635 eV below the CB.[15] V_O^* is ~0.86 eV below the CB and V_O^{++} is 1.16 eV above the VB,[27] for a typical band gap of 3.36 eV (ref.[16]) The CB and VB locations are taken from Ref [61]. Numerals (1) through (5) represent PCA that can take place at different places.

Table 1 Spectral locations of deconvoluted peaks and ascribed emission mechanism. The wavelength of the emission is given in nm, and eV for convenience.

Sample	Interband (nm, eV)	V_{Zn} or Zn_i related (nm, eV)		V_O related (nm, eV)	
PZ1 QD	382, 3.25 (a_1)	400, 3.10 (b_1)	433, 2.86 (c_1)	501, 2.47 (d_1)	564, 2.20 (e_1)
PZ2 NC	386, 3.21 (a_2)	404, 3.06 (b_2)	432, 2.87 (c_2)	498, 2.49 (d_2)	565, 2.20 (e_2)
PZ3 NC	390, 3.18 (a_3)	407, 3.04 (b_3)	436, 2.85 (c_3)	499, 2.49 (d_3)	562, 2.21 (e_3)
PZ4 NC	389, 3.19 (a_4)	407, 3.04 (b_4)	437, 2.83 (c_4)	500, 2.48 (d_4)	566, 2.19 (e_4)
Mechanism	$\mathbf{FX} \xrightarrow{395\ nm} \mathbf{VB}$	$\mathbf{Zn_i} \xrightarrow{395\ nm} \mathbf{VB}$ $\mathrm{CB} \xrightarrow{405\ nm} V_{Zn}$	$\mathbf{ex\text{-}Zn_i} \xrightarrow{440-455\ nm} \mathbf{VB}$ $\mathrm{Zn}_i \xrightarrow{437\ nm} V_{Zn}$	$\boldsymbol{V_O^*} \xrightarrow{500\ nm} \mathbf{VB}$	$\mathbf{CB} \xrightarrow{564\ nm} \boldsymbol{V_O^{++}}$

Finally, to comment on the overall defect density and their predominance, the emission due to V_Os is gradually increasing where the intensity due to Zn_i is almost stable. This is very significant finding [15] where it is believed that the obtaining a balance between V_Os and Zn_is is rather hard task, i.e. if the density of Zn_i increases than that of V_Os decreases.

To further justify the existence Zn_is, their origin and their balance against V_Os needs to be considered. The relative concentration of these defects is strongly dependent on formation temperature as their ionization energies lie in the range of ~0.05 to 2.8 eV.[33] In the case of vapor phase deposition, the partial pressure and their relative pressures of zinc and oxygen are also found to be vital [37,62] and as expected under highly reducing environment together with high temperatures causes V_Os to dominate [37] or under zinc rich environments Zn_is are the predominant defects. Under high temperature (~1100˚C) annealing of ZnO crystals depicted Zn_is.[40] Therefore, the chosen parameters of ALD has yielded high densities of Zn_is, where the duration of the precursor pulse, substrate and its temperature are believed to be detrimental.

Since we have employed different cycle numbers to manipulate the morphology, the amount of ZnO is quantified from TGA thermograms (see Fig. S5 of ESI and its explanation). The weight percentages of ZnO in the PSU-ZnO fibers were calculated by subtracting the char yield (%) of the pristine PSU fibers at 700˚C

yielding 10, 14, 19 and 25 % in PZ1 QD, PZ 2 NC, PZ 3 NC and PZ4 NC respectively. PCA on MB in the presence of PSU-ZnO samples was tested under UV-illumination of 365 nm wavelength; as a result, *electrons* are excited to CB rather any defect sites. The degradation of MB (C/C_0) as a function of 't' is plotted in Fig. 8a. We have observed exponential decay behavior which falls into pseudo-first-order kinetics as explained by Langmuir-Hinshelwood model. Note that the degradation follows[1] Langmuir sorption isotherms,[63] in which organic molecules are adsorbed on the surface as a monolayer at a distance of 1 Å. These adsorbed molecules are oxidized through a process mediated by hydroxyl radical (·OH).[2,3] This ·OH radical forms either from *electron* [3] (at CB or defect site) via molecular oxygen or from *hole* [2] (at VB or defect site) via adsorbed H_2O or OH^- groups on the surface. The mechanism that govern these processes are given in Eq (6) and (7) after Izumi et al.[3] and Matthews.[2] Please refer to our earlier articles [4,8] for the detailed discussion involving the equations (6) and (7). Note that the oxidation involves the charge carrier from semiconductor, hence one needs to balance the interfacial charge transfer between the semiconductor and dye against carrier recombination to achieve higher efficiencies.

$$\left.\begin{array}{c} e^-_{CB} + O_2 \rightarrow {}^{\cdot}O_2^- \\ {}^{\cdot}O_2^- + H^+ \rightarrow {}^{\cdot}HO_2 \\ 2\,{}^{\cdot}HO_2 \rightarrow H_2O_2 + O_2 \\ {}^{\cdot}O_2^- + {}^{\cdot}HO_2 \rightarrow {}^{\cdot}HO_2^- + O_2 \\ {}^{\cdot}HO_2^- + H^+ \rightarrow H_2O_2 \\ H_2O_2 + {}^{\cdot}O_2^- \rightarrow {}^{\cdot}OH + OH^- + O_2 \text{ (or)} \\ H_2O_2 + e^-_{CB} \rightarrow {}^{\cdot}OH + OH^- \text{ (or)} \\ H_2O_2 \xrightarrow{h\nu} 2\,{}^{\cdot}OH \end{array}\right] ----(6)$$

$$\left.\begin{array}{c} h^+_{VB} + H_2O \rightarrow {}^{\cdot}OH + H^+ \\ h^+_{VB} + HO^- \rightarrow {}^{\cdot}OH \end{array}\right] ----(7)$$

In the no catalyst and PSU cases no degradation is observed within the UV exposure, in contrast, PSU-ZnO samples have shown a finite decay time of varying spans (Fig. 8a). Equations (6) and (7) govern the PCA on the surface of ZnO, where the defect sites play a crucial role in trapping the charge carriers. Please refer to Fig. 7b for the energetic location of each defect with reference to CB and VB of ZnO, where the active sites for PCA are indicated with numerals, (1) through (5). Zn_i, and ex-Zn_i can capture *electrons* from CB and can take part in PCA. Although V_O^* exists in the bulk of the grain, however, it depicts indirect effect by capturing an *electron* from CB there by delaying the recombination process. Hence due to V_O^*, PCA takes place at VB via *hole*. On the other hand V_O^{++} exists in the DR, which may be available for PCA, showing enhanced effect when compared to V_O^*. This is because V_O^{++} can be on the surface or at grain boundaries where the captured *hole* and the delayed *electron* at CB can participate in PCA.

As mentioned in the introduction, we aim to elucidate the effect of Zn_is and V_Os on the PCA. In order to achieve this we have compared the activities and the percentage increase for each defect density (area under the peaks of $a_{1\text{-}4}$ through $e_{1\text{-}4}$ corresponding to each defect type) is calculated (please refer to the description in the Table S2 legend of ESI) with reference to PZ1 QD which were correspondingly annotated as primed alphabets (Fig. 8b). Also note that if *electron* is captured by a defect, the associated *hole* at VB takes part in catalysis. Conversely, if *hole* is captured by a defect then, *electron* in CB can take part in catalysis. The percentage decrease in τ is also calculated with reference to that of PZ1 QD ($[\tau_{PZ1\ QD}\text{-}\tau_{PZ2,\ 3\ or\ 4\ NC}]*100/\tau_{PZ1\ QD}$) and shown on Fig. 8c. By taking into account of the discussion on relative densities of various defects, in the following we will attribute the difference in τ for PSU-ZnO samples referring to Fig. 8b and c. Notably, PZ1 QD has shown longer τ than the others (Fig. 8a). However, the percentage decrement of τ suggests an improvement in performance of ~77 % for PZ2 NC. This increment is cumulative from various defects as expected. PZ1 QD is predominant with ex-Zn_is hence the PCA takes place at (2) and (3) in addition to (1) and (5) (Fig. 8b). In the case of PZ2 NC, Zn_is are as dense as PZ1 QD sample while ex-Zn_i states are subdued. On the other hand a' and e' are almost doubled, which enhance the PCA at (1), (5) and (1), (4) respectively. b_2 emission is slightly improved while ignoring that of d_2. Hence, majorly the ~77 % improvement is a sum effect of contribution from a' [(1), (5)], e' [(1), (4)] and b' [(2), (5)] in that order. If similarly argued, the following conclusions can be drawn for the rest of the samples. PZ1 QD to PZ3 NC an improvement of ~80 % is noticed. This is a sum effect of contribution from e' [(1), (4)], d' [(5)], a' [(1), (5)] and b' [(2), (5)] in that order. Finally, PZ1 QD to PZ4 NC an improvement of ~88 % is noticed which is a sum effect of contribution from e' [(1), (4)], d' [(5)], a' [(1), (5)] and b' [(2), (5)] in that order. As discussed earlier, the physical location of V_Os suggests that for the same defect levels of e' and d', the former shows higher PCA than the latter. By given the overall scenario, the important thing to note is that the PCA is not severely affected by defect density above a certain degree. For example, PZ1 QD to PZ3 NC, the net increase in the defect density is nearly 770 %; however, the PCA has shown an improvement from 77 to 80 %. On the other hand, PZ1 QD to PZ2 NC, the net increase in the defect density is 200 % which has shown 77% improvement in PCA. Although the ex-Zn_is have subdued, the increased optical quality and V_O^{++} states have shown an improvement of 77 % in PCA, which is a significant finding. Despite of such great contribution from V_Os it is notable that further increase in their density did not help to enhance the PCA. However, it is convincing that V_Os enhance the PCA,[4,8,10,11,13,21] which can probably dominate the contribution from Zn_is and/or ex-Zn_is. This is because of the differences in the intrinsic nature of the defects. From equations (1) through and (5) it appears that both the Zn_i and V_Os can form ionized levels, however in the earlier explanation by Zeng et al.[15] there is no discussion on charged zinc interstitials forming defect bands within the band gap. In clear contrast to this, V_Os form two defect levels [17,27,64,65] within the band gap by following the equations (4) and (5). Among these two bands although one is not directly accessible for PCA, it shows an indirect effect by capturing an *electron* from CB. Furthermore, equation (5) is feasible [17,27] in the DR of the semiconductor, where the obvious places on the surface are the grain boundaries. As the thickness increases, initially grains takes shape along with grain boundaries where the latter are very favorable places for the dye to adsorb. As evidenced in XPS, V_Os are occupied by oxygen related functional groups, which can be, for example, –OH, H_2O and/or O_2. These species can participate and/or mediate the PCA directly. Although the point of zero charge for ZnO is 9.0 ± 0.3, due to the predominance of V_Os the surface of ZnO can be negatively charged in the presence of –OH groups, which are more favorable for the cationic dye like MB. In the present context we did not consider the pH of the solution and its effects. Also note (equation (7)) that the PCA involving H_2O is associated with h_{VB}^+ forming the most reactive hydroxyl radical (E^0 = +3.06 V) where the *holes* can be captured by V_O^+. In our earlier study [4] we have given further explanation why *holes* are more reactive than *electrons*. Hence by given the above reasons, it is concluded that Zn_is are less reactive than V_Os.

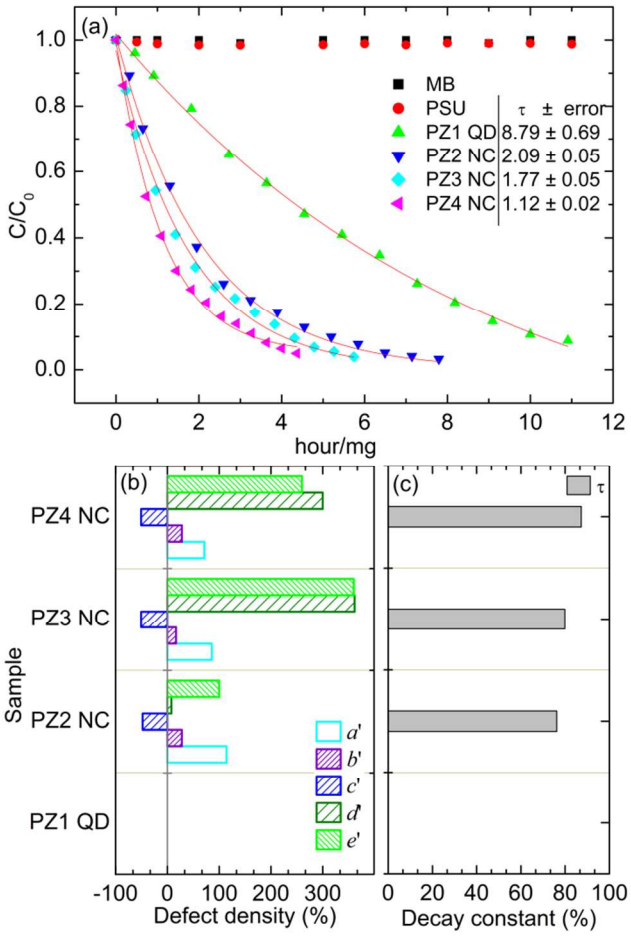

Fig. 8 (a) PCA of various samples compared with pristine PSU and no catalyst cases, (b) densities of various defects and (c) improvement in decay constant are referenced with PZ1 QD case and shown in percentage.

Conclusions

We have fabricated ZnO QDs on the surface of electrospun PSU fibers and carefully investigated the changes in the properties when QDs transform into NC when ALD cycles are increased. Since polymers are known for their flexibility, PSU-ZnO fibers were no exception in ease handling, as shown in Fig. S6 of ESI. The morphological characterization suggested that the ALD precursors and PSU are well compatible. The growth rate of ZnO film is determined to be ~0.2 nm/cycle. The morphological transformation has shown significant variance in the crystal and optical properties of the samples. The average size of the ZnO QDs is determined to be around 10 nm from TEM micrograms. SAED patterns were recorded and a representative pattern to be identified as polycrystalline ZnO. Apart from the confirmation of wurtzite structure, the XRD data suggested that the samples have suffered from severe strain, which might be due to the intrinsic lattice defects. XPS has evidenced Zn_i related defects quite explicitly for PZ1 QD sample. This is because of non-uniform molecular adsorption of H_2O vapor on surface of PSU to react with DEZn. The PL spectra are recorded for all the samples, and the probable transitions are recognized based on the available evidence in line with literature. Interestingly, PZ1 QD has shown nominal signature of V_Os from XPS which is consistent with PL data. Significantly, the increase in the density of V_Os occurred for higher ALD cycle numbers, *viz* ≥ 300 for almost the same density of Zn_is. The PCA experiment is performed on the samples which depicted pseudo first order kinetics. The decay constant is estimated for all PSU-ZnO samples via first order exponential fit. The fitting outputs of PL spectra are employed to estimate the relative densities of Zn_is and V_Os by considering the area under each peak corresponding to the defect related transitions. The percent improvement in PCA is juxtaposed against the defect densities. The results suggest that Zn_is and related defects are less efficient than V_Os in the context of photocatalysis. This is mainly because of the accessibility of these defects for the PCA. Both of Zn_i and V_O capture charge carriers thereby delaying the recombination process, however, the intrinsic nature of V_O allow them to exist in the grain boundaries (V_O^{++}) where the region is depleted with charge carriers and in the bulk of the grain (V_O^{*}). Trapped *hole* at V_O^{++} consequently an *electron* is delayed at CB can participate in the PCA in addition to delayed hole at VB due to V_O^{*}. This double effect is not seen in the case of Zn_is which makes them less efficient when compared to V_Os.

Acknowledgements

F.K. thanks TUBITAK-BIDEB for a PhD scholarship. S.V. thanks The Scientific & Technological Research Council of Turkey (TUBITAK) (TUBITAK-BIDEB 2221 - Fellowships for Visiting Scientists and Scientists on Sabbatical) for fellowship. N.B. thanks EU FP7-Marie Curie-IRG for funding NEMSmart (PIRG05-GA-2009-249196). T.U. thanks EU FP7-Marie Curie-IRG NANOWEB (PIRG06-GA-2009-256428) and The Turkish Academy of Sciences - Outstanding Young Scientists Award Program (TUBA-GEBIP) for partial funding. Authors thank M. Guler for technical support for TEM analysis.

.

Notes and references

[a] UNAM-National Nanotechnology Research Centre, Bilkent University, Ankara, 06800, Turkey.
[b] Institute of Materials Science & Nanotechnology, Bilkent University, Ankara, 06800, Turkey.
SV: svempati01@qub.ac.uk; TU: uyar@unam.bilkent.edu.tr

† Electronic Supplementary Information (ESI) available: Distribution of particle sizes, NC thickness comparison, XRD, fluorescence spectra, TGA and digital photographs. See DOI: 10.1039/b000000x/

1 M. R. Hoffmann, S. T. Martin, W. Choi and D. Bahnemann, *Chem. Rev.*, 1995, **95**, 69-96.
2 R. W. Matthews, *J. Catal.*, 1986, **97**, 565-568.
3 I. Izumi, W. W. Dunn, K. O. Wilbourn, F. R. F. Fan and A. J. Bard, *J. Phys. Chem.*, 1980, **84**, 3207-3210.
4 F. Kayaci, S. Vempati, C. Ozgit, I. Donmez, N. Biyikli and T. Uyar, *Nanoscale*, 2014, DOI:10.1039/C1033NR06665G.
5 N. Zhang and Y.-J. Xu, *Chem. Mater.*, 2013, **25**, 1979-1988.
6 N. Zhang, S. Liu and Y.-J. Xu, *Nanoscale*, 2012, **4**, 2227-2238.
7 C. Yu, K. Yang, Y. Xie, Q. Fan, J. C. Yu, Q. Shu and C. Wang, *Nanoscale*, 2013, **5**, 2142-2151.

8 F. Kayaci, S. Vempati, C.O.-Akgun, N. Biyikli and T. Uyar, *Accepted Appl. Catal. B.*, 2014.
9 H. Tada, T. Kiyonaga and S. Naya, *Chem. Soc. Rev.*, 2009, **38**, 1849-1858.
10 I. Nakamura, N. Negishi, S. Kutsuna, T. Ihara, S. Sugihara and K. Takeuchi, *J. Mol. Catal.A*, 2000, **161**, 205–212.
11 X. Pan, M.-Q. Yang, X. Fu, N. Zhang and Y.-J. Xu, *Nanoscale*, 2013, **5**, 3601-3614.
12 M. K. Nowotny, L. R. Sheppard, T. Bak and J. Nowotny, *J.Phys. Chem. C*, 2008, **112**, 5275.
13 J. Wang, P. Liu, X. Fu, Z. Li, W. Han and X. Wang, *Langmuir*, 2009, **25**, 1218-1223.
14 C. Yu, G. Li, S. Kumar, K. Yang and R. Jin, *Adv. Mater.*, 2013, **26**, 892-898.
15 H. Zeng, G. Duan, Y. Li, S. Yang, X. Xu and W. Cai, *Adv. Funct. Mater.*, 2010, **20**, 561.
16 S. Vempati, J. Mitra and P. Dawson, *Nanoscale Res. Lett.*, 2012, **7**, 470.
17 S. Vempati, S. Chirakkara, J. Mitra, P. Dawson, K. K. Nanda and S. B. Krupanidhi, *Appl. Phys. Lett.*, 2012, **100**, 162104.
18 *Vacancies on cation and anion sublattices can be paired to form neutral (Schottky) defect, or a vacancy can be compensated by an interstitial of same atom. A paired vacancy and interstitial can also form a neutral defect (Frenkel).Hence the ionicity of intrinsic defect is controlled by the lattice, in contrast to doping where a successful doping depends on the ionicity of the dopant.*
19 F. Kayaci, C. Ozgit-Akgun, N. Biyikli and T. Uyar, *RSC Adv.*, 2013, **3**, 6817-6820.
20 F. Kayaci, C. Ozgit-Akgun, I. Donmez, N. Biyikli and T. Uyar, *ACS Appl. Mater. Interfaces*, 2012, **4**, 6185-6194.
21 H. Liu, J. Yang, J. Liang, Y. Huang and C. Tang, *J. Am. Ceram. Soc.*, 2008, **91**, 1287-1291.
22 A. Sugunan, V. K. Guduru, A. Uheida, M. S. Toprak and M. Muhammed, *J. Am. Ceram. Soc.*, 2010, **93**, 3740–3744.
23 N. Zhang, Y. Zhang and Y.-J. Xu, *Nanoscale*, 2012, **4**, 5792.
24 K. T. Johnson, T. E. Gribb, E. M. Smoak and I. A. Banerjee, *Chemical Communications*, 2010, **46**, 1757-1759.
25 U. Ozgur, Y. Alivov, C. Liu, A. Teke, M. Reshchikov, S. Dogan, V. Avrutin, S. Cho and H. Morkoc, *J. Appl. Phys.*, 2005, **98**, 041301.
26 L. Schmide-Mende and J. L. MacManus-Driscoll, *Mater. Today*, 2007, **10**, 40.
27 J. D. Ye, S. L. Gu, F. Qin, S. M. Zhu, S. M. Liu, X. Zhou, W. Liu, L. Q. Hu, R. Zhang, Y. Shi and Y. D. Zheng, *Appl. Phys. A: Mater. Sci. Process.*, 2005, **81**, 759-762.
28 W. H. Zhang, J. L. Shi, L. Z. Wang and S. S. Yan, *Chem. Mater.*, 2000, **12**, 1408.
29 E. G. Bylander, *J. Appl. Phys.*, 1978, **49**, 1188.
30 J. J. Wu and S. C. Liu, *Adv. Mater.*, 2002, **14**, 215.
31 S. Vempati, A. Shetty, P. Dawson, K. Nanda and S. B. Krupanidhi, *J. Cryst. Growth*, 2012, **343**, 7-12.
32 S. Vempati, A. Shetty, P. Dawson, K. K. Nanda and S. B. Krupanidhi, *Thin Solid Films*, 2012, **524**, 137-143.
33 L. S. Vlasenko and G. D. Watkins, *Phys. Rev. B*, 2005, **72**, 035203.
34 A. Janotti and C. G. V. d. Walle, *Phys. Rev. B*, 2007, **76**, 165202.
35 H. B. Zeng, W. P. Cai, Y. Li, J. L. Hu and P. S. Liu, *J. Phys. Chem. B*, 2005, **109**, 18260.
36 H. B. Zeng, Z. G. Li, W. P. Cai, B. Q. Cao, P. S. Liu and S. K. Yang, *J. Phys. Chem. B*, 2007, **111**, 14311.
37 K. I. Hagemark and L. C. Chacha, *J. Solid State Chem.* , 1975, **15**, 261.
38 G. W. Tomlins, J. L. Routbort and T. O. Mason, *J. Appl. Phys.*, 2000, **87**, 117.
39 B. J. Wuensch and H. L. Tuller, *J. Phys. Chem. Solids*, 1994, **55**, 975.
40 J. P. Han, P. Q. Mantas and A. M. R. Senos, *J. Eur. Ceram. Soc.*, 2002, **22**, 49.
41 L. E. Halliburton, N. C. Giles, N. Y. Garces, M. Luo, C. C. Xu, L. H. Bai and L. A. Boatner, *Appl. Phys. Lett.*, 2005, **87**, 172108.
42 T. Uyar, R. Havelund, J. Hacaloglu, F. Besenbacher and P. Kingshott, *ACS Nano* 2010, **4**, 5121.
43 S. Agarwal, A. Greiner and J. H. Wendorff, *Adv. Funct. Mater.*, 2009, **19**, 2863.
44 M. E. Fragalà, I. Cacciotti, Y. Aleeva, R. L. Nigro, A. Bianco, G. Malandrino, C. Spinella, G. Pezzotti and G. Gusmano, *Cryst. Eng. Comm.*, 2010, **12**, 3858.
45 B. Gong and G. N. Parsons, *J. Mater. Chem.*, 2012, **22**, 15672.
46 J. S. Jur, W. J. Sweet III, C. J. Oldham and G. N. Parsons, *Advanced Functional Materials*, 2011, **21**, 1993-2002.
47 M. Kemell, V. Pore, M. Ritala, M. Leskelä and M. Lindén, *J. Am. Chem. Soc.* , 2005, **127**, 14178.
48 R. L. Puurunen, *J. Appl. Phys.*, 2005, **97**, 121301.
49 C. J. Oldham, B. Gong, J. C. Spagnola, J. S. Jur, K. J. Senecal, T. A. Godfrey and G. N. Parsons, *J. Electrochem. Soc.*, 2011, **158**, D549-D556.
50 V. Ischenko, S. Polarz, D. Grote, V. Stavarache, K. Fink and M. Driess, *Adv. Funct. Mater.*, 2005, **15**, 1945.
51 *NIST X-ray Photoelectron Spectroscopy Database, Version 4.1 (National Institute of Standards and Technology, Gaithersburg, 2012); http://srdata.nist.gov/xps/.*
52 M. Chen, X. Wang, Y. Yu, Z. Pei, X. Bai, C. Sun, R. Huang and L. Wen, *Appl. Surf. Sci.*, 2000, **158**, 134-140.
53 A. Stănoiu, C. E. Simion and S. Somăcescu, *Sens. Actu. B: Chem.*, 2013, **186**, 687-694.
54 D. C. Look and J. W. Hemsky, *Phys. Rev. Lett.*, 1999, **82**, 2552.
55 F. Tuomisto, V. Ranki, K. Saarinen and D. C. Look, *Phys. Rev. Lett.*, 2003, **91**, 205502.
56 D. C. Look, G. C. Falow, P. Reunchan, S. Limpijumnong, S. B. Zhang and K. Nordlund, *Phys. Rev. Lett.*, 2005, **95**, 225502.
57 C. H. Ahn, Y. Y. Kim, D. C. Kim, S. K. Mohanta and H. K. Cho, *J. Appl. Phys.*, 2009, **105**, 013502.
58 S.-H. Jeong, B.-S. Kim and B.-T. Lee, *Appl. Phys. Lett.*, 2003, **82**, 2625.
59 B. Lin, Z. Fu and Y. Jia, *Appl. Phys. Lett.*, 2001, **79**, 943.
60 P. S. Xu, Y. M. Sun, C. S. Shi, F. Q. Xu and H. B. Pan, *Nucl. Instrum. Methods B*, 2003, **199**, 286-290.
61 L. Ley, R. A. Pollak, F. R. McFeely, S. P. Kowalczyk and D. A. Shirley, *Phys. Rev. B*, 1974, **9**, 600-621.
62 F. Oba, S. R. Nishitani, S. Isotani and H. Adachi, *J. Appl. Phys.*, 2001, **90**.
63 I. Langmuir, *J. Am. Chem. Soc.*, 1918, **40**, 1361-1403.

64 A. v. Dijken, E. A. Meulenkamp, D. Vanmaekelbergh and A. Meijerink, *J. Lumin.*, 2000, **90**, 123-128.
65 K. Vanheusden, W. L. Warren, C. H. Seager, D. R. Tallant, J. A. Voigt and B. E. Gnade, *J. Appl. Phys.*, 1996, **79**, 7983.